nuclei and subsequently added WGA to seal the existing pores. A nucleoplasmic signal was detectable when these nuclei were stained with αNup133 and αNup160 (*24*). In contrast to mock-depleted cytosol, Nup107-160–depleted cytosol did not induce the assembly of new pores (Fig. 3C). This lack of activity was caused by the absence of Nup107-160, because the addition of purified Nup107-160 complex (fig. S2C) restored NPC insertion (Fig. 3C).

Nuclei were formed in the presence of BAPTA (1,2-bis(2-aminophenoxy)ethane-*N*,*N*,*N*′,*N*′-tetraacetic acid), a calcium chelator that inhibits NPC formation (*25*), and a strong nucleoplasmic Nup133 signal was detected (Fig. 3D). When the BAPTA nuclei were diluted in mock-depleted cytosol, NPC insertion was restored, whereas Nup107-160–depleted cytosol failed to do so (Fig. 3D). Consistent with the cytoplasmic RanGTP-mediated release of Importin β from the Nup107-160 complex, we found that the addition of 5 μM RanT24N resulted in a 60% increase of Importin β associated with immunoprecipitated Nup107-160 complex (*24*). Thus, the incorporation of the Nup107-160 complex into new assembly sites occurs from both sides of the NE. Because nuclear transport is not required for NPC insertion in vitro, the nucleoplasmic pool of Nup107-160 complexes might be generated via chromatin association during nuclear assembly (*17*).

Next we wanted to analyze if pores assemble de novo or by the splitting of existing pores (*7–9*). We assembled NE-0 nuclei and subsequently fluorescently labeled individual pores with WGA-488 (green) (Fig. 4A). Upon dilution, WGA-488 remained stably bound to NPCs while new unlabeled pores were inserted (fig. S3A), which could be labeled with WGA-568 (red). Newly formed pores were only labeled with WGA-568 and appeared as red dots, whereas old pores were labeled with both dyes resulting in a yellow overlay. The new pores did not exhibit green signal from existing pores, suggesting that NPCs form de novo (Fig. 4A). When the formation of new pores was blocked by the addition of 5 μM RanT24N, all pores appeared yellow in the overlay (Fig. 4A), indicating that red dots represented newly formed pores. Furthermore, the average fluorescence intensity of WGA-488–labeled NPCs remained constant after dilution of the dye, and it was indistinguishable between nuclei that inserted new pores and nuclei where the formation of new NPCs was blocked by 5 μM RanT24N (fig. S3B). These results suggest that newly formed pores do not incorporate nucleoporins from existing NPCs, and they support a de novo mechanism, because in a splitting process, the intensity of the old pores would be expected to decrease. Additionally, we were able to detect pores that stained with αPOM121, a transmembrane nucleoporin, and Nup133,

but not with mAb414 (fig. S3C). POM121 colocalized with mAb414 when the formation of new NPCs was blocked by RanT24N (fig. S3C). This indicates that phenyl-glycyl–repeat nucleoporins are recruited to new assembly sites after POM121 and Nup107-160 complexes have been incorporated and further supports de novo formation.

To determine whether NPC formation in vivo also occurs by a de novo mechanism, we generated a stable HeLa cell line expressing low, nontoxic levels of POM121 containing multiple copies of green fluorescent protein (GFP) to visualize individual NPCs in living cells (*26*). Four-dimensional confocal time-lapse microscopy was used to follow NPC assembly during interphase and new pores became visible as single dots in areas where initially no GFP signal was detectable (Fig. 4B and Movie S1) and in areas where preexisting pores have been photobleached (Fig. 4D). New NPCs colocalized with neighboring, preexisting pores along the z axis (fig. S4, A and B), showing that they were inserted into the NE. Consistent with de novo formation, existing pores did not change fluorescence intensity over time (Fig. 4C). These findings further support a de novo mechanism for NPC biogenesis.

References and Notes

1. S. R. Wente, *Science* **288**, 1374 (2000).
2. D. Gorlich, U. Kutay, *Annu. Rev. Cell Dev. Biol.* **15**, 607 (1999).
3. G. G. Maul, L. L. Deaven, J. J. Freed, G. L. Campbell, W. Becak, *Cytogenet. Cell Genet.* **26**, 175 (1980).
4. G. G. Maul *et al.*, *J. Cell Biol.* **55**, 433 (1972).
5. M. Winey, D. Yarar, T. H. Giddings Jr., D. N. Mastronarde, *Mol. Biol. Cell* **8**, 2119 (1997).
6. B. Burke, J. Ellenberg, *Nat. Rev. Mol. Cell Biol.* **3**, 487 (2002).
7. M. Hetzer, T. C. Walther, I. W. Mattaj, *Annu. Rev. Cell Dev. Biol.* (2005).
8. K. Bodoor *et al.*, *Biochem. Cell Biol.* **77**, 321 (1999).
9. G. Rabut, P. Lenart, J. Ellenberg, *Curr. Opin. Cell Biol.* **16**, 314 (2004).
10. M. J. Lohka, Y. Masui, *Science* **220**, 719 (1983).
11. M. Hetzer, D. Bilbao-Cortes, T. C. Walther, O. J. Gruss, I. W. Mattaj, *Mol. Cell* **5**, 1013 (2000).
12. L. I. Davis, G. Blobel, *Proc. Natl. Acad. Sci. U.S.A.* **84**, 7552 (1987).
13. M. Dasso, *Curr. Biol.* **12**, R502 (2002).
14. C. Klebe, H. Prinz, A. Wittinghofer, R. S. Goody, *Biochemistry* **34**, 12543 (1995).
15. D. R. Finlay, E. Meier, P. Bradley, J. Horecka, D. J. Forbes, *J. Cell Biol.* **114**, 169 (1991).
16. A. Harel *et al.*, *Mol. Biol. Cell* **14**, 4387 (2003).
17. T. C. Walther *et al.*, *Nature* **424**, 689 (2003).
18. F. R. Bischoff, C. Klebe, J. Kretschmer, A. Wittinghofer, H. Ponstingl, *Proc. Natl. Acad. Sci. U.S.A.* **91**, 2587 (1994).
19. C. Klebe, F. R. Bischoff, H. Ponstingl, A. Wittinghofer, *Biochemistry* **34**, 639 (1995).
20. D. Gorlich, *Curr. Opin. Cell Biol.* **9**, 412 (1997).
21. K. J. Ryan, J. M. McCaffery, S. R. Wente, *J. Cell Biol.* **160**, 1041 (2003).
22. A. Harel *et al.*, *Mol. Cell* **11**, 853 (2003).
23. T. C. Walther *et al.*, *Cell* **113**, 195 (2003).
24. M. A. D'Angelo, D. J. Anderson, E. Richard, M. W. Hetzer, data not shown.
25. C. Macaulay, D. J. Forbes, *J. Cell Biol.* **132**, 5 (1996).
26. N. Daigle *et al.*, *J. Cell Biol.* **154**, 71 (2001).
27. M. Hetzer *et al.*, *Nat. Cell Biol.* **3**, 1086 (2001).
28. Materials and methods are available as supporting material on *Science* Online.
29. G. Rabut, V. Doye, J. Ellenberg, *Nat. Cell Biol.* **6**, 1114 (2004).
30. Antibodies against Importin β were kindly provided by L. Gerace. We thank the members of our laboratory and T. Hunter for helpful discussions and W. Eckhart, J. Karlseder, V. Lundblad, J. Young, B. Sefton, and M. Weitzman for critically reading the manuscript. M.A.D and M.H. were supported by The Pew Charitable Trust.

Differential Targeting of Gβγ-Subunit Signaling with Small Molecules

Tabetha M. Bonacci,[1] Jennifer L. Mathews,[1] Chujun Yuan,[2] David M. Lehmann,[1] Sundeep Malik,[1] Dianqing Wu,[3] Jose L. Font,[1] Jean M. Bidlack,[1] Alan V. Smrcka[1,2]*

G protein βγ subunits have potential as a target for therapeutic treatment of a number of diseases. We performed virtual docking of a small-molecule library to a site on Gβγ subunits that mediates protein interactions. We hypothesized that differential targeting of this surface could allow for selective modulation of Gβγ subunit functions. Several compounds bound to Gβγ subunits with affinities from 0.1 to 60 μM and selectively modulated functional Gβγ-protein-protein interactions in vitro, chemotactic peptide signaling pathways in HL-60 leukocytes, and opioid receptor–dependent analgesia in vivo. These data demonstrate an approach for modulation of G protein–coupled receptor signaling that may represent an important therapeutic strategy.

The βγ subunits of heterotrimeric guanine nucleotide binding proteins (G proteins) are released upon ligand activation of G protein–coupled receptors (GPCRs). Free Gβγ subunits bind and regulate multiple target proteins within the cell—including phospholipase C (PLC) β2 and PLC β3, phosphoinositide 3 kinase (PI3K) γ, adenylyl cyclase, N-type Ca^{2+} channels, and inwardly rectifying K^+ channels—and mediate physiological

processes such as neutrophil chemotaxis, vascular cell proliferation, and cardiac chronotropy (*1*, *2*).

To investigate the molecular nature of Gβγ-target recognition, we screened random-peptide phage display libraries for binding to $G\beta_1\gamma_2$ and identified a series of peptides that bound to a single preferred protein-protein interaction surface ("hotspot") on Gβ (*3*). One of the peptides (SIRK) blocked Gβγ-dependent regulation of PLCβ2 and PI3Kγ but not regulation of type I adenylyl cyclase or N-type Ca^{2+} channels, thus demonstrating the potential for selective targeting of Gβγ signaling. The crystal structure of $G\beta_1\gamma_2$ in a complex with a SIRK peptide derivative (SIGK) reveals the preferred interaction surface as a region overlapping the Gα-switch II domain binding surface on top of the Gβ propeller (*4*–*6*). Subclasses of peptides appeared to bind distinct subsurfaces of the hotspot and differentially affect G protein subunit interactions. Many Gβγ effectors also use diverse mechanisms for binding within this surface (*7*, *8*), and because peptides showed some selectivity, we hypothesized that small organic molecules also might selectively modulate Gβγ-target interactions.

We used FlexX virtual screening software (*9*) in the Sybyl molecular modeling package to dock 1990 compounds in the chemical diversity set from the National Cancer Institute (NCI) to the interaction hotspot of $G\beta_1\gamma_2$. The diversity library was designed to contain chemical core structures representative of the larger 250,251-compound library from NCI. The docked models were ranked using five scoring functions in C-Score: D-score, G-score, F-score, Chemscore, and PMF-score (*10*). Two consensus scores that equally weight the five scoring functions were also used to rank the compounds. The top 1% of compounds from each scoring function (85 compounds total) were tested for their ability to compete with phage-displaying SIGK for binding to biotinylated $G\beta_1\gamma_2$ ($bG\beta_1\gamma_2$) in an enzyme-linked immunosorbent assay (ELISA) (*3*). Nine of the 85 compounds inhibited SIGK binding with median inhibitory concentration (IC_{50}) values ranging from 100 nM to 60 μM (Fig. 1B and table S1).

One compound, M119, with a high apparent affinity for $bG\beta_1\gamma_2$ (ELISA IC_{50} = 200 nM) (Fig. 1, B and C, and table S1) was selected as a lead to define structure-activity requirements (SAR) for binding to $G\beta_1\gamma_2$.

Twenty-one compounds from the NCI library with similar structures to M119 were tested for relative $G\beta_1\gamma_2$ binding affinities (Fig. 1C and table S2). For example, the apparent affinity of M119B for $bG\beta_1\gamma_2$ is $1/1000$ that of M119, with the key chemical difference being the loss of two hydroxyl groups. Thus, specific chemical characteristics may be required for interactions with the Gβγ hotspot. We next tested whether M119 could disrupt protein interactions with a bona fide Gβγ binding partner, $G\alpha_{i1}$. The hotspot for protein interaction overlaps with the Gα switch II binding surface on Gβγ. The overall $G\alpha_{i1}$-βγ interaction surface spans 1800 Å² (*5*, *6*), and the dissociation constant (K_d) for $G\alpha_{i1}$ binding to Gβγ is ~1 nM (*11*). M119 competed with fluorescein isothiocyanate (FITC)–α_{i1} ($F\alpha_i$) for binding to $bG\beta_1\gamma_2$ with an IC_{50} value of 400 nM (Fig. 1D). However, unlike SIGK and related peptides that bind to this surface (*12*), M119 did not promote dissociation of $G\alpha_i$ from Gβγ (fig. S1).

FlexX docking software predicted that compounds M201 and M119 (Fig. 1C) bound to distinct subsurfaces in the hotspot, but M201 did not compete for SIGK binding. Nevertheless, we tested M119 and M201 in in vitro reconstitution assays of Gβγ-dependent activation of PLCβ2, PLCβ3, and PI3Kγ and binding to GRK2. M119 attenuated $G\beta_1\gamma_2$-dependent activation of PLCβ2 (IC_{50} value of 3 μM), PLCβ3, and PI3Kγ (Fig. 2, A to C, left panels). M201, on the other hand, did not affect PLCβ2 activation by $G\beta_1\gamma_2$ but potentiated $G\beta_1\gamma_2$-dependent activation of both PLCβ3 and PI3Kγ (Fig. 2, A to C, right panels). M119 also inhibited direct binding of $bG\beta_1\gamma_2$ to PLCβ2 and PLCβ3, whereas M201 did not block binding of PLCβ2 and enhanced binding of PLCβ3 to $G\beta_1\gamma_2$ (fig. S2). M119 and M201 both inhibited GRK2 binding to $bG\beta_1\gamma_2$ with similar IC_{50} values of approximately 5 μM (Fig. 2D). A weakly binding compound M119B (Fig. 1C and table S2) did not have effects in these assays (fig. S3). These
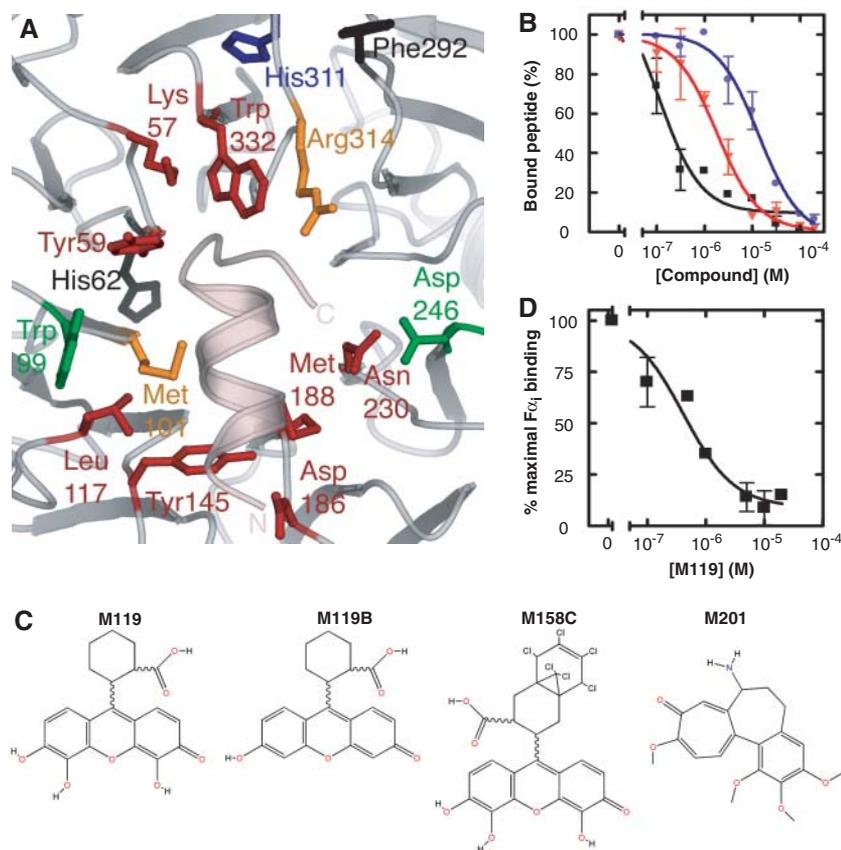

Fig. 1. Small molecule binding to the hotspot on Gβγ. (**A**) Structure of SIGK bound to Gβγ at the hotspot. Amino acids within 6.5 Å of SIGK were targeted with the FlexX module of Sybyl virtual docking software. (**B**) Competition ELISA data for three of the compounds identified in the virtual screen. Compounds were tested for their ability to inhibit binding of a phage displaying the peptide SIGKAFKILGYPDYD (*3*, *4*). M119 (NSC119910) (squares); M109 (NSC109208) (triangles); M117 (NSC117079) (circles). Data for all the binding compounds are summarized in table S1. (**C**) Structures of representative βγ-binding compounds. (**D**) Competition of M119 for interactions between $G\alpha_{i1}$ and $G\beta_1\gamma_2$. F-α_{i1} and M119 were simultaneously added to $bG\beta_1\gamma_2$ immobilized on streptavidin beads. The amount of bead-based fluorescence was assessed by flow cytometry as described (*11*, *12*).

[1]Department of Pharmacology and Physiology and [2]Department of Biochemistry and Biophysics, University of Rochester School of Medicine and Dentistry, Rochester, NY 14642, USA. [3]Department of Genetics and Developmental Biology, University of Connecticut Health Center, Farmington, CT 06030, USA.

*To whom correspondence should be addressed. E-mail: Alan_Smrcka@URMC.rochester.edu

data suggest that both M201 and M119 bind to Gβγ but differentially modulate Gβγ interactions with effectors. These are only two of multiple diverse compounds identified, which suggests the potential for multiple modes of Gβγ-dependent target modulation by these small molecules.

To test the effects of differentially targeting Gβγ on GPCR signaling in intact cells, M119 (and a similar compound, M158C) (Fig. 1C and table S2) and M201 were tested for their ability to modulate fMLP receptor–dependent signaling in differentiated HL-60 leukocytes. The fMLP receptor couples to Gi in these cells and activates PLCβ2 (PLCβ3 is a minor isoform in these cells), PI3Kγ, and ERK through Gβγ signaling (13, 14). Pretreatment of differentiated HL-60 cells with M119 and M158C (Fig. 3A and fig. S4A), but not M201 (Fig. 3B and

fig. S4B), attenuated fMLP-induced Ca^{2+} increases. M119 had no effect on carbachol-dependent increases in Ca^{2+} in HEK293 cells stably expressing the Gq-linked M3-muscarinic receptor, confirming a specific effect of M119 on Gβγ-dependent Ca^{2+} mobilization (fig. S4C). fMLP-dependent GRK2 translocation to the membrane fraction of HL-60 cells, on the other hand, was substantially inhibited by incubation with either M119 or M201 (Fig. 3C). Thus, M119 and M201 differentially modulate PLCβ2 regulation by Gβγ, yet both inhibit GRK2 binding in intact cells.

To assess the ability of M119 and M158C to inhibit fMLP receptor–dependent regulation of PI3Kγ activation, we stimulated HL-60 cells stably overexpressing a green fluorescent protein (GFP)–tagged pleckstrin homology (PH) domain from Akt (15) with fMLP and assessed

translocation of the GFP-PHAkt to the membrane by subcellular fractionation and Western blotting. The PH domain from Akt binds to PIP_3 produced by PI3K activity at the membrane. Pretreatment of the cells with 10 μM of M119 or M158C inhibited fMLP-dependent translocation of GFP-PHAkt to the membrane (Fig. 3D), consistent with the ability of these compounds to inhibit activation of PI3Kγ by Gβγ.

Stimulation of differentiated HL-60 cells with fMLP also results in pertussis toxin–sensitive activation of various MAP kinases, including ERK1 and ERK2, p38, and JNK (16). However, pretreatment of HL-60 cells with M119, M158C, and M201 did not block fMLP-induced activation of ERK1 and ERK2 (Fig. 3E). Ca^{2+} mobilization occurred at low fMLP (100 nM) concentrations relative to that required to observe ERK1 and ERK2 (1 μM) activation, indicating that the selective lack of effect of M119 on ERK activation is not due to excess G protein activation.

We tested the efficacy of our compounds in an in vivo model. Compared with wild-type animals, $PLC\beta3^{-/-}$ mice are 10 times as sensitive to the antinociceptive effects of the μ-agonist morphine (17). Because M119 blocks Gβγ-dependent activation of PLCβ3, we tested whether coadministration of M119 with morphine would also increase morphine-induced antinociception. Coadministration of M119 with morphine intracerebroventricularly resulted in an 11-fold increase in the analgesic potency of morphine (Fig. 4A) [ED_{50} values and 95% confidence limits: 0.069 (0.023 to 0.201) nmol and 0.743 (0.341 to 1.62) nmol, respectively], whereas administration of 100 nmol M119 alone had no effect on baseline antinociception (table S3). M119 also had no effect on morphine-dependent antinociception in $PLC\beta3^{-/-}$ mice (Fig. 4B). These data highlight the specificity of M119 actions and the selective nature of M119 both in vitro and in vivo. Gβγ subunits regulate many aspects of signaling critical for the actions of opioid agonists (18). If M119 were globally blocking Gβγ subunit functions, we expect that morphine-induced antinociception would have been attenuated rather than potentiated with M119 coadministration.

Protein interaction interfaces present difficult drug targets because of the generally large interaction surface area and flat topology of the interaction surfaces. Hotspots at protein interfaces comprise a small fraction of the overall interaction surface, yet are responsible for most of the energetics of binding, and it has been proposed that targeting such surfaces could successfully disrupt protein-protein binding (19). As a result of extensive screening, some protein interaction interfaces have been targeted with small molecules (19–21). Our screen of only 1990 molecules identified multiple compounds with apparent affinities in the high nM

Fig. 2. Differential effects of M119 and M201 on βγ-dependent regulation of downstream targets. (**A**) Effects of M119 and M201 (NSC201400) on Gβγ-activation of PLCβ. Purified PLCβ2 (0.25 ng) was assayed in the presence (triangles) or absence (squares) of 100 nM purified $G\beta_1\gamma_2$. (**B**) Effects of M119 and M201 effects on purified PLCβ3 (0.5 ng) activity in the presence (triangles) or absence (squares) of 100 nM purified $G\beta_1\gamma_2$. (**C**) Effects of M119 and M201 on activation of PI3Kγ by $G\beta_1\gamma_2$. Assays contained 10 ng of purified p101/p110 PI3Kγ heterodimer with or without 100 nM purified $G\beta_1\gamma_2$. Left,: (triangles) 100 nM $G\beta_1\gamma_2$ or (squares) no βγ. (**D**) Effects of M119 and M201 on Gβγ-GRK2 interactions. M119 or M201 and 25 nM purified GRK2 were added simultaneously to 250 nM $bG\beta_1\gamma_2$ immobilized on streptavidin agarose. Associated GRK2 was detected with antibody to GRK2. Data are representative experiments [mean ± SEM, except (D)] and were repeated at least three times each. The concentrations of compound required for these assays are apparently higher than predicted by the phage ELISA assays, but may reflect the different assay conditions and protein concentrations required for each assay.
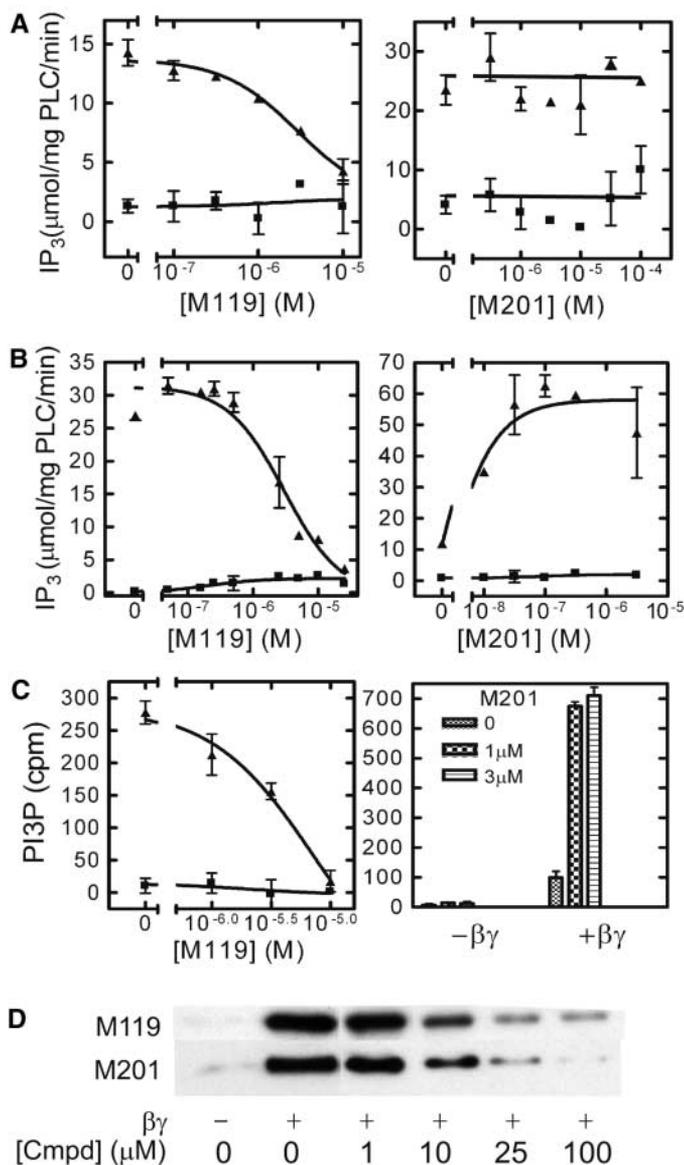
Fig. 3. Effects of M119 and related compounds on Gβγ signaling in dimethyl sulfoxide (DMSO)–differentiated HL-60 cells. (**A**) M119 and related compounds block fMLP-dependent Ca²⁺ release in differentiated HL-60 cells, loaded with 1 μM Fura2-AM. Cells were pretreated with DMSO or 10 μM compounds for 5 min before stimulation with 250 nM fMLP. The change in fluorescence was monitored at 340/380 nm. Data are representative of five independent experiments. Compounds are significantly different than DMSO control, $P < 0.01$. See fig. S4A for dose dependence. (**B**) Same as A except 10 μM M201 was tested. Data are representative of four independent experiments. See fig. S4B for pooled data. (**C**) M119 and M201 inhibition of GRK2 translocation. Differentiated HL-60 cells were treated with 10 μM compound before stimulation with 250 nM fMLP. Translocation of endogenous GRK2 was determined by Western blotting with a GRK2 antibody and quantitative chemiluminescence. Data are mean ± SEM from five experiments, $*P < 0.05$, $**P < 0.01$ analysis of variance (ANOVA). (**D**) M119 and M158C (NSC158110) inhibition of GFP-PHAkt translocation. Differentiated HL-60 cells stably overexpressing GFP-PHAkt were treated with 10 μM compound before stimulation with 100 nM fMLP. Translocation of GFP-PHAkt to the membrane was determined by Western blotting with antibody to GFP and quantitative chemiluminescence. Data are mean ± SEM from four experiments. $***P < 0.001$ ANOVA. (**E**) Lack of effect of M119, M158C, and M201 on fMLP-induced ERK1 and ERK2 activation. Differentiated HL-60 cells were pretreated with 10 μM of compound prior to stimulation with 1 μM fMLP for 5 min. Levels of phosphorylated and total ERK were determined by Western blotting. This experiment was repeated three times with similar results.
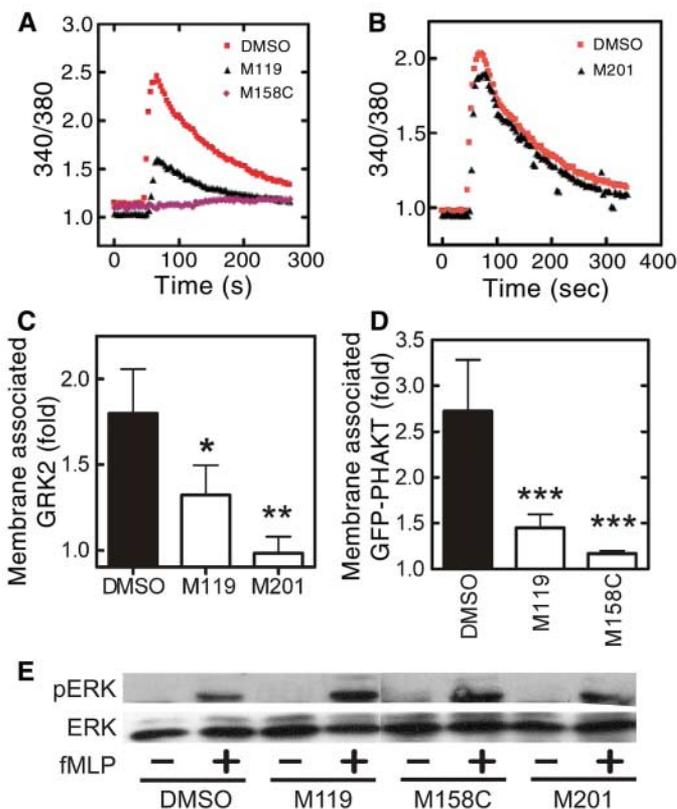

Fig. 4. M119 effects on morphine-induced antinociception in (**A**) wild-type and (**B**) PLCβ3⁻/⁻ mice. Increasing concentrations of morphine were administered intra-cerebroventricularly to mice with (squares) or without (triangles) concomitant administration of 100 nmol M119. Antinociception was measured 20 min after injection using the 55°C tail-flick test. Data are mean ± SEM from 7 to 10 animals at each point.
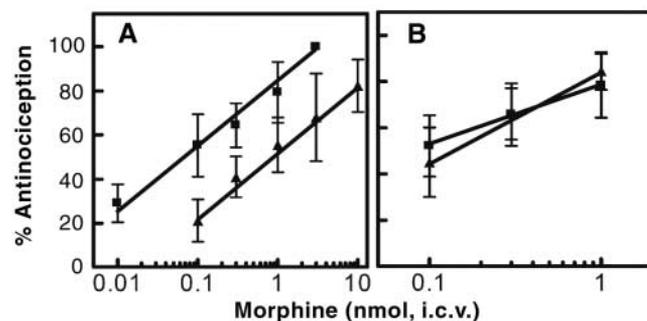
to low μM range. These molecules demonstrate that multiple small molecule binders of Gβγ could be developed that differentially modulate functions downstream of GPCRs. Numerous studies in animal models have implicated Gβγ-subunit targeting as a therapeutic strategy in diseases such as heart failure (*22*), prostate cancer (*23*), vascular disease (*24*), and inflammatory disease (*13*). Thus, more extensive screening for molecules that bind to the Gβγ hotspot will yield a repertoire of potentially therapeutically useful small molecules.

References and Notes
1. D. E. Clapham, E. J. Neer, *Annu. Rev. Pharmacol. Toxicol.* **37**, 167 (1997).
2. T. M. Cabrera-Vera *et al.*, *Endocr. Rev.* **24**, 765 (2003).
3. J. K. Scott *et al.*, *EMBO J.* **20**, 767 (2001).
4. T. Davis, T. M. Bonacci, A. V. Smrcka, S. R. Sprang, *Biochem.* **44**, 10593 (2005).
5. M. A. Wall *et al.*, *Cell* **83**, 1047 (1995).
6. D. G. Lambright *et al.*, *Nature* **379**, 311 (1996).
7. C. E. Ford *et al.*, *Science* **280**, 1271 (1998).
8. Y. Li *et al.*, *J. Biol. Chem.* **273**, 16265 (1998).
9. M. Rarey, B. Kramer, T. Lengauer, G. Klebe, *J. Mol. Biol.* **261**, 470 (1996).
10. R. D. Clark, A. Strizhev, J. M. Leonard, J. F. Blake, J. B. Matthew, *J. Mol. Graph. Model.* **20**, 281 (2002).
11. N. A. Sarvazyan, A. E. Remmers, R. R. Neubig, *J. Biol. Chem.* **273**, 7934 (1998).
12. M. Ghosh, Y. K. Peterson, S. M. Lanier, A. V. Smrcka, *J. Biol. Chem.* **273**, 34747 (2003).
13. Z. Li *et al.*, *Science* **287**, 1046 (2000).
14. E. R. Neptune, H. R. Bourne, *Proc. Natl. Acad. Sci. U.S.A.* **94**, 14489 (1997).
15. G. Servant *et al.*, *Science* **287**, 1037 (2000).
16. M. J. Rane, S. L. Carrithers, J. M. Arthur, J. B. Klein, K. R. McLeish, *J. Immunol.* **159**, 5070 (1997).
17. W. Xie *et al.*, *Proc. Natl. Acad. Sci. U.S.A.* **96**, 10385 (1999).
18. M. Connor, M. J. Christie, *Clin. Exp. Pharmacol. Physiol.* **26**, 493 (1999).
19. M. R. Arkin, J. A. Wells, *Nat. Rev. Drug Discov.* **3**, 301 (2004).
20. A. G. Cochran, *Curr. Opin. Chem. Biol.* **5**, 654 (2001).
21. T. Oltersdorf *et al.*, *Nature* **435**, 677 (2005).
22. G. Iaccarino, W. J. Koch, *Assay Drug Dev. Technol.* **1**, 347 (2003).
23. Y. Daaka, *Sci. STKE* **2004**, re2 (2004).
24. G. Iaccarino, L. A. Smithwick, R. J. Lefkowitz, W. J. Koch, *Proc. Natl. Acad. Sci. U.S.A.* **96**, 3945 (1999).
25. We thank the Developmental Therapeutics Program at the NCI/NIH for providing the compounds used in this study, J. Benovic for providing purified GRK2, H. Bourne for providing HL-60 cells stably overexpressing GFP-PHAkt, and S. Sprang for evaluation of this manuscript. Supported by NIH grants GM60286 (A.V.S.), K05-DA00360 (J.M.B.), HL080706 (D.W.), Predoctoral Training grant in Cardiovascular Biology HL-T3207949 (T.M.B.), and NIDA Drug Abuse Training grant T32DA07232 (J.L.M.).

Science

Differential Targeting of Gßγ-Subunit Signaling with Small Molecules

Tabetha M. Bonacci, Jennifer L. Mathews, Chujun Yuan, David M. Lehmann, Sundeep Malik, Dianqing Wu, Jose L. Font, Jean M. Bidlack and Alan V. Smrcka

ARTICLE TOOLS	http://science.sciencemag.org/content/312/5772/443
SUPPLEMENTARY MATERIALS	http://science.sciencemag.org/content/suppl/2006/04/18/312.5772.443.DC1
RELATED CONTENT	http://science.sciencemag.org/content/sci/312/5772/377.full http://stke.sciencemag.org/contenthttp://stke.sciencemag.org/cgi/content/abstract/sigtrans;2006/332/tw140 http://stke.sciencemag.org/content/sigtrans/2006/332/tw140.abstract
REFERENCES	This article cites 24 articles, 11 of which you can access for free http://science.sciencemag.org/content/312/5772/443#BIBL
PERMISSIONS	http://www.sciencemag.org/help/reprints-and-permissions

Use of this article is subject to the Terms of Service